Structural Engineering and Mechanics, *Vol. 63, No. 4 (2017) 521-536*
DOI: https://doi.org/10.12989/sem.2017.63.4.521

Earthquake effects on the energy demand of tall reinforced concrete walls with buckling-restrained brace outriggers

Hamid Beiraghi*

Department of Civil Engineering, Mahdishahr Branch, Islamic Azad University, Mahdishahr, Iran

(Received December 6, 2016, Revised May 19, 2017, Accepted June 5, 2017)

Abstract. Reinforced concrete core-wall structures with buckling-restrained brace outriggers are interesting systems which have the ability to absorb and dissipate energy during strong earthquakes. Outriggers can change the energy demand in a tall building. In this paper, the energy demand was studied by using the nonlinear time history analysis for the mentioned systems. First, the structures were designed according to the prescriptive codes. In the dynamic analysis, three approaches for the core-wall were investigated: single plastic hinge (SPH), three plastic hinge (TPH) and extended plastic hinge (EPH). For SPH approach, only one plastic hinge is allowed at the core-wall base. For TPH approach, three plastic hinges are allowed, one at the base and two others at the upper levels. For EPH approach, the plasticity can extend anywhere in the wall. The kinetic, elastic strain, inelastic and damping energy demand subjected to forward directivity near-fault and ordinary far-fault earthquakes were studied. In SPH approach for all near-fault and far-fault events, on average, more than 65 percent of inelastic energy is absorbed by buckling-restrained braces in outrigger. While in TPH and EPH approaches, outrigger contribution to inelastic energy demand is reduced. The contribution of outrigger to inelastic energy absorption for the TPH and EPH approaches does not differ significantly. The values are approximately 25 and 30 percent, respectively.

Keywords: near-fault; earthquake; reinforced concrete wall; buckling-restrained brace; outrigger; energy

1. Introduction

Earthquake loads in tall buildings usually cause significant displacements due to large shear forces. In up to 40-story buildings, all seismic lateral loads can be carried only by a core-wall system. For taller buildings, outriggers usually can mitigate the deformations (Rahgozar *et al.* 2009). Numerous researchers have carried out investigations on structure responses with damped outriggers. Zhou and Li (2013) investigated the numerical dynamic response of outrigger systems subjected to seismic loads. They concluded that the increase of earthquake intensity makes the influence of viscous damper more obvious. Bobby *et al.* (2014) developed a performance-based topology optimization analysis for wind sensitive tall buildings. Chen *et al.* (2010) investigated a simplified model with two viscous dampers attached to the end of outriggers and studied the optimum location and damping coefficient of the damper. Buckling-restrained brace (BRB) is relatively a new type of brace that can be used in the outriggers to dissipate energy. Response of frames with BRBs has been investigated by researchers (Fanaie *et al.* 2014). The study of energy in tall core-wall systems with BRB outriggers is an interesting and new issue (Bosco *et al.* 2013).

The codes recommend the use of reduced lateral forces in design and therefore permit nonlinear deformation in the predefined region of the wall (Marzban *et al.* 2014, Esmaili *et al.* 2011). Traditionally, plastic hinges in cantilever RC walls occur preferably in the flexure at the base of the wall (Paulay *et al.* 1992). In the dual plastic hinge approach, the formation of more than one plastic hinge is allowed in the reinforced concrete (RC) core-wall (Panagiotou and Restrepo 2009).

Forward directivity (pulse-like) ground motions may cause large deformation and strength demands in structures and consequently increase the damage compared to the ordinary far-fault (FF) motions (Haselton *et al.* 2011, Liel *et al.* 2011, Eskandari *et al.* 2015, Beiraghi *et al.* 2016a, Eskandari *et al.* 2017, Vafaei *et al.* 2010, Vafaei and Eskandari 2015, 2016). This effect has been recognized as one of the major characteristics of near-fault (NF) ground motions that cause extensive structural damages. Getting away from the causative fault, the effect of forward directivity decreases in the seismic waves, such that near-fault pulse-like ground motions are unlikely to take place in distances larger than 10 to 15 km away from the rupture (Iervolino *et al.* 2008).

The near-fault motion specification depends on the shaking intensity, fault geometry and the orientation of the earthquake waves (Mortezaei *et al.* 2013, Somerville 1997). Generally, the pulse existing in the velocity time history is more prevalent than in the acceleration or displacement records. In earthquake engineering, the velocity pulse is a more popular indicator of damage than the acceleration pulse. The damage potential and earthquake-induced collapse risks are also associated with the maximum displacement during the near-fault pulse-like ground motions (Hall *et al.* 1995).

*Corresponding author, Ph.D.
E-mail: h.beiraghi@msh-iau.ac.ir

ISSN: 1225-4568 (Print), 1598-6217 (Online)

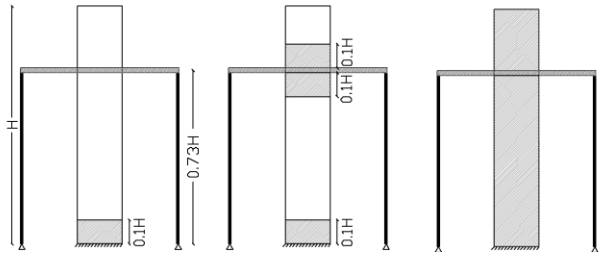

Fig. 1 SPH, TPH and EPH approaches for the core-wall (plasticity can extend in the hatched area)

The concept of energy has been an interesting subject for the researchers to improve seismic resistant design approach since 1950s (Housner *et al.* 1956, Massumi *et al.* 2013). Energy-based approach can form the basis of estimating expected seismic demands and can indirectly predict the destructive potential of ground motions. Methodologies developed by considering the input and dissipated energy have been proposed by some researchers (Fajfar *et al.* 1992, Teran-Gilmore *et al.* 1998, Riddell *et al.* 2001).

The energy input of structures due to various earthquake ground motions has been measured by some researchers (Uang and Bertero 1997, Kuwamura and Galambos 1989). These studies indicated the possibility of hysteretic energy input as a useful parameter for explaining structural demands and damages.

Energy demand is considered as a reliable tool for the prediction of seismic hazard. The energy method is seen as a reliable assessment of the demand of the dissipated energy and is dependent on the earthquake characteristics. Numerous researchers implemented this assessment by means of the evaluation of the input energy (Uang *et al.* 1990).

As a result of the instantaneous energy demand associated with extreme pulse effects and few nonlinear cycles, Near-fault earthquakes can cause large damages. In the Near-fault events, the effects of low-cycle fatigue are almost insignificant, and structural damage is more affected by peak seismic demands. Records having significant acceleration pulses produce sudden energy rise in the early phase of response, which can be considerably larger than the energy accumulated at the end (Kalkan and Kunnath 2006).

Forward directivity near-fault records have so unique properties that can cause a structure to dissipate earthquake input energy in a few large plastic cycles. It seems that the investigation of energy demand and its variation during an earthquake, as well as the investigation of structural properties, may lead to a more precise understanding of seismic demands in the earthquakes (Kalkan and Kunnath 2006, Beiraghi *et al.* 2016b).

Earthquake input energy is a suitable intensity measure for near-fault type of ground motions (Luco *et al.* 2007). This parameter accounts not only for the ground motion specification, like duration or frequency content of motions, but also for the structural properties such as ductility, damping, and hysteretic behavior. Therefore, it is an appropriate measure of earthquake intensity, compared to other parameters such as Peak Ground Acceleration or Spectral Intensity used by some researchers (Khashaee *et al.* 2003).

So far, the energy demands for tall RC core-wall buildings with BRB outriggers subjected to the NF and FF earthquake records have not been investigated. BRB outriggers can change the deformation and energy demand of core-walls over the height and cause the formation of a new plastic hinge over the core-wall height. In this paper, the outrigger-core-wall structures were designed using the traditional response spectrum analysis (RSA). To investigate the dynamic behavior, three approaches were examined. In the single plastic hinge (SPH) approach, only one plastic hinge is allowed to form at the base of the core-wall and the remaining region of the core-wall is maintained in the elastic limit. In the three plastic hinge (TPH) approach, in addition to the base plastic hinge, two other plastic hinges in the core-wall, adjacent to above and below of the outrigger level is allowed, and the remaining area of the core-wall is maintained in the elastic limit. In the extended plastic hinge (EPH) approach, plasticity can extend anywhere in the core-wall. In all the three approaches, the BRB outrigger experiences a nonlinear deformation. The nonlinear time history analysis of the systems was carried out and the corresponding energy demands were investigated. The concepts of SPH, TPH and EPH approaches are represented in Fig. 1. SPH and TPH approaches required ductile detail for 10% and 30% of the core-wall, respectively; while EPH approach required ductile detail for all the height.

2. Structural design

In this study, 40-, 50- and 60-story structures with a typical story height of 3.5 m were taken into consideration. For design purposes, three-dimensional linear elastic finite element models of the core-wall, outrigger and connected columns to the outriggers were generated in ETABS software (2015 version 15.1.0). The floor was made of RC slabs. The negligible effect of the columns only carrying gravity load on the seismic responses has been demonstrated by Calugaru *et al*. (2012), previously. Selection of the outrigger level has been described in another paper (Beiraghi and Siahpolo 2017). Based on the software, the shell-type plate elements were used to model the shear wall. This type of element utilizes a triangular or quadrilateral formulation which combines the separate membrane and plate-bending behaviors. There are six deformation components for the element nodes. The distributed dead and live loads of the floors were assigned as 7 and $2\frac{\mathrm{KN}}{\mathrm{m}^2}$, respectively. The tributary dead and live loads carried by the core-wall and the outside columns were assigned to each of them. The mass of each story was assigned to the center of mass of the floors in the models, and a rigid diaphragm was used. The base of the core-wall is fixed, while the base of the column is pinned type. All the lateral seismic loads applied on the structure were carried by the core-wall, outrigger and connected columns. A Linear design of all the structures was accomplished using

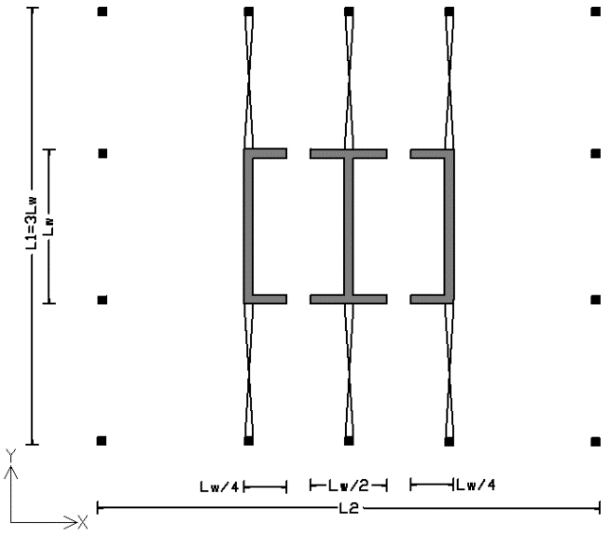

Fig. 2 Typical plan of the studied systems

RSA procedure at design basis earthquake (DBE) level. Designing of the models was carried out based on the ASCE 7 (2010), ACI 318 (2011) and AISC (2005) Codes. A response modification factor equal to 5 was used as recommended by the NEHRP Seismic Design Technical Brief No. 6 (2012). The lateral design forces were scaled to 85% of the base shear which was calculated according to the equivalent static base shear procedure. The typical plan of the building is presented in Fig. 2. Similar core-wall plans have been used in the real structures (Klemencic *et al.* 2007).

The peripheral columns were made of steel material and the outrigger consisted of BRBs. The connection between beams and columns and also between BRBs and other elements were pinned connection.

To account for the concrete cracks, a reduction factor equal to 0.5 was applied. This reduction factor was used to reduce the flexural stiffness of the core-wall and its value is in accordance with the stiffness reduction factors recommended in the ACI 318-2011(Sections 8.8 and 10.10).

The yielding strength of the steel applied in column was 370 MPa. The nominal yielding strength of the steel reinforcement and the nominal compression strength of the concrete were 400 and 45 MPa, respectively. Approximately more than 96% of the modal participating mass ratio results from the first 4 translational vibrational modes in the Y direction. It should be noted that all the analyses and designs were limited to the Y direction. In the core-wall, the minimum longitudinal reinforcement ratio was 0.25% (ACI 318-2011). The vertical steel reinforcement distribution in each floor was uniform and the nominal flexural strength at each level was greater than the calculated design moment envelope. The boundary element length was in accordance with the ACI 318 and was extended to 10, 7, and 3% of the wall height from the base for the 40-, 50- and 60-story buildings, respectively. As shown in Table 1, the longitudinal reinforcement ratio throughout every 10% of the height remained constant. For all considered models, the ratio of total height to the L1 was 4.67 (Fig. 2).

Table 1 Calculated longitudinal reinforcement for the *RC* core-wall

40 ST		50 ST		60 ST	
No. of story	Reinforcing ratio	No. of story	Reinforcing ratio	No. of story	Reinforcing ratio
1-4	1.27	1-5	1.48	1-6	1.72
5-8	0.63	6-10	0.57	7-12	0.45
9-12	0.25	11-15	0.25	13-18	0.25
13-16	0.25	16-20	0.25	19-24	0.25
17-19	0.25	21-25	0.25	25-30	0.25
20-21	0.25	26-30	0.4	31-37	0.27
22-24	0.52	31-35	0.77	38-43	0.57
25-28	0.9	36-37	0.64	44-46	0.52
29-30	0.78	38-42	0.68	47-52	0.57
31-34	0.62	43-47	0.35	52-60	0.25
35-40	0.28	48-50	0.25	-	-

Table 2 Structural specifications of designed buildings

Total number of stories	40	50	60
Building height (m)	140	175	210
Core-Wall length (*Y* direction), L_w (m)	10	12.5	15
Floor plan dimension ($L1\times L2$) (m)	30×35	37.5×42.5	45×50
Core-Wall thickness (m)	0.5	0.75	1.15
Outrigger stories no.	29,30	36,37	44,45,46
Brace cross-section area (m^2)	0.0430	0.0748	0.1239
Total seismic weight of structure (ton)	37000	75000	138000
Gravity load ratio of core-wall at base (*P/Agfc*)	0.155	0.18	0.197
Normalized height of outrigger level (from base)	0.73	0.73	0.74
Design base shear (ton)	2150	4480	8390
*T*1 (sec) (*Y* direction)	4.42	5.66	6.64
*T*2 (sec) (*Y* direction)	0.91	1.12	1.26
*T*3 (sec) (*Y* direction)	0.41	0.47	0.50

To design the BRB braces, axial forces calculated through the modal response spectrum analysis were reduced by an assigned value of the response modification factor. The capacity of the braces in tension and compression were both formulized as $\varphi A_s F_y$, where A_s is the cross section of the brace element, and φ and F_y equal to 0.9 and 250 MPa, respectively. (Sahoo *et al.* 2010).

According to the AISC's Seismic Provisions for Structural Steel Buildings (AISC-2005), two items for columns in buckling restrained braced frames need to be checked: first, the axial load and moment interaction for code level forces; second, the axial load only corresponding to the sum of the vertical component of all buckling restrained braces applied to the column along with tributary gravity loads. For the columns of considered models, the second criterion governed the design and produced larger demand/capacity ratios. The maximum expected compression forces from the brace are calculated as

Table 3 Calculated cross-section area for columns conn ected to the outriggers

40 ST		50 ST		60 ST	
No. of story	Column cross-section (m^2)	No. of story	Column cross-section (m^2)	No. of story	Column cross-section (m^2)
1-10	0.2624	1-18	0.2944	1-20	0.3424
11-30	0.2304	19-37	0.2624	21-46	0.2624
31-40	0.1320	38-50	0.1551	47-60	0.1776

$R_y\omega\beta A_s F_y$, where R_y, the material over strength equals 1.1, ω, the strain-hardening effect equals 1.25 and β, the compression over-strength factor equals 1.1 (Jones *et al.* 2009). Tables 2 and 3 show the specification of the structures designed using the code prescriptive approach.

3. Inelastic modeling

An assessment of the building responses was accomplished using nonlinear models in Perform-3D software (Perform-3D V4 2011) subjected to seismic loads. The columns and beams were modeled with elastic members. After each analysis, the elastic behavior of these elements was checked through controlling the demand/capacity ratio. A rigid diaphragm was used for the structure floors and the mass property was assigned to each floor at the center of mass. The length of each plastic hinge of the RC core-wall in the SPH and TPH approaches is 0.1H (Panagiotou and Restrepo 2009).

3.1 Fiber element verification

The ability of fiber element method to simulate RC shear wall response has been demonstrated by some researchers (Orakcal *et al.* 2006). In one research, the result of an experimental program (Ghorbanirenani *et al.* 2012) was used to investigate the accuracy of the numerical shear wall element in Perform-3D software. The tested RC wall was an 8-story shear wall subjected to the base shaking vibration. The NLTHA was performed to calculate the responses of numerical model. The responses obtained from the verified model showed a good agreement with the values measured by the experimental work. More information of the verification was presented in another paper (Beiraghi *et al.* 2015).

3.2 BRB component model

A bar-type element that resists axial force only and has no resistance to torsional or bending forces is available in Perform-3D as BRB component. In BRB component, there exist a linear portion which is incapable of yielding and a nonlinear portion which is capable of yielding; hence the component consists of two bars in series. The length of the restrained nonlinear portion of a BRB component is assumed to be 0.7 of the node-to-node brace element length. The remaining 30% is assumed as the linear portion that is the non-yielding portion. Generally, the linear portion consists of the transition and the end segment (Fig. 3). The cross section area of the transition and end segment of BRBs are taken larger than the restrained nonlinear portion to prevent yielding of the linear portion. The cross section area of transition and end segments (A_t and A_e) of the BRB elements used were 1.6 and 2.2 times the cross section area of the core cross section, respectively. Also, the length of the transition and end segments were chosen as 0.06 and 0.24 times the total length of the bracing (Nguyen *et al.* 2011).

To calculate the cross section area of the yielding core (A_c) of the BRB element, the following equation was used (Bosco *et al.* 2013)

$$\frac{L_c}{A_c} = \frac{L_w}{A_{eq}} - \frac{L_e}{A_e} - \frac{L_t}{A_t} \quad (1)$$

Where L_c, L_t, L_e and L_w represent the lengths of the yielding core, transition segment, end segment and the whole bracing, respectively; Also, A_{eq} is the cross section area of the equivalent bar calculated from the linear design procedure. Fig. 4 shows the hysteretic response for the BRB element used in the nonlinear model (Simpson *et al.* 2009).

3.3 Nonlinear fiber for assumed systems

In this study, the nonlinear behavior of core-wall models was estimated using a fiber element approach in Perform-3D software. The verification for the fiber wall elements

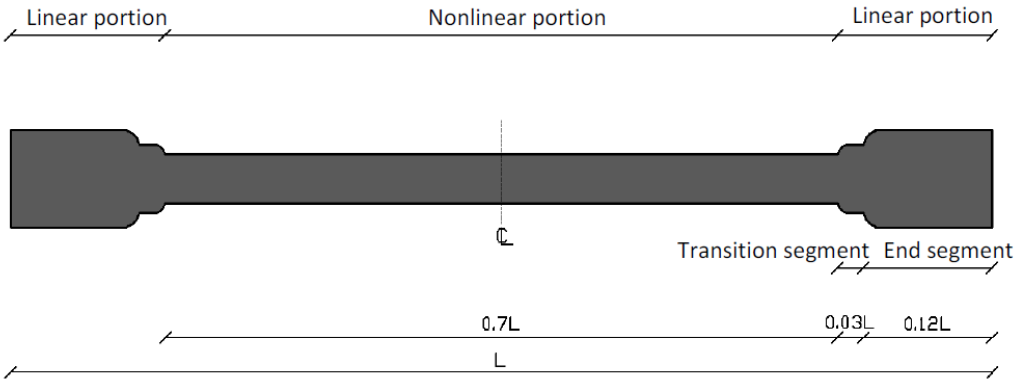

Fig. 3 Schematic view of a BRB portions (Beiraghi and Siahpolo 2017)

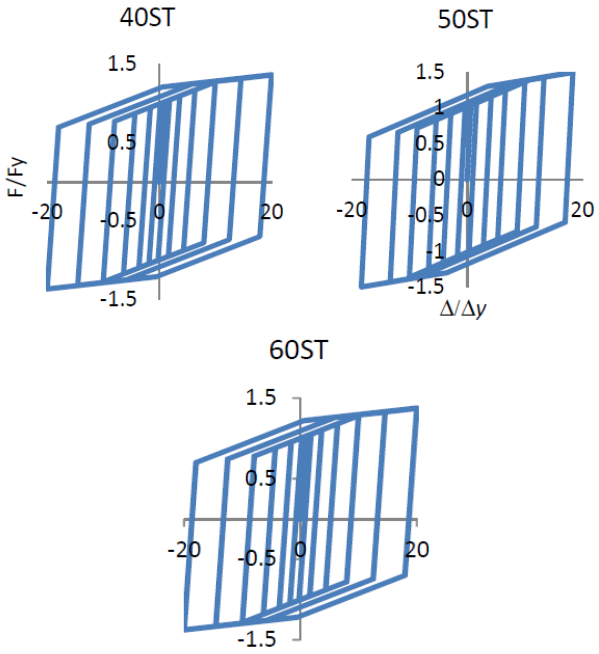

Fig. 4 Hysteretic response of the BRBs used in the numerical models (horizontal axis is axial displacement to yielding displacement and vertical axis is axial force to yielding force ratio)

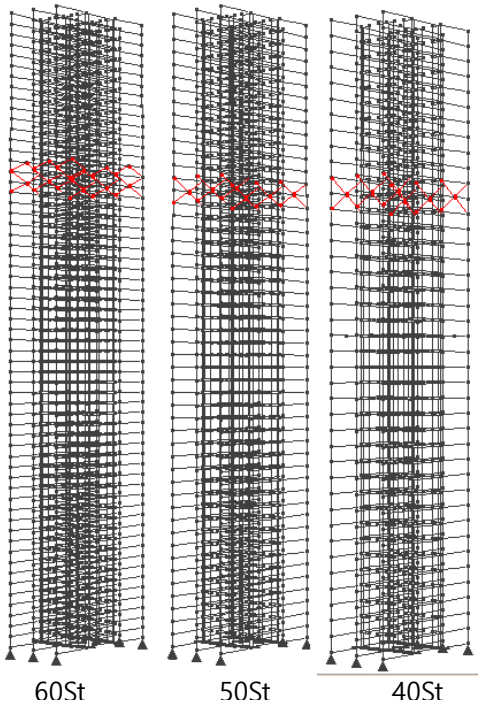

Fig. 5 The three-dimensional numerical model of the lateral load resisting systems

was described in section 3.1. Each fiber wall element utilizes 4 nodes and 24 degrees of freedom (Perform-3D user guide, 2006). Each fiber element cross-section comprises the vertical steel and concrete fibers. Nonlinear concrete fiber uses a strain-stress model of confined concrete based on the modified Mander model (Mander *et al.* 1988). The tensile strength of the concrete was ignored. The expected concrete compressive strength is 1.3 times the specified strength used for design. The expected yield strength of the steel bars is 1.17 times its nominal yield strength (LATBSDC 2014). The strength and stiffness degradation in RC wall element are applied by specifying the degradation factor for longitudinal reinforcements. This factor considers the ratio of the degraded to non-degraded hysteresis loop area (Ghodsi *et al.* 2010). In each story, one element was used to simulate each RC wall component (Powell, 2007). Fig. 5 shows the perspective view of the numerical models for NLTHA. The shear behavior of the wall elements was assumed to be linear elastic. A typical value for shear stiffness is from GcAg/20 to GcAg/10, as recommended by ATC72 (2010). In this study, the value of GcAg/15 was used for shear stiffness, where GcAg indicates the elastic shear stiffness.

3.4 Ground motion records

Ground motions are used to conduct time history analyses of buildings with the objective of understanding the response of a structure during earthquake, from the energy point of view. Time history analyses were conducted using multiple ground motion records. For the NF ground motions, due to the special pattern of shear deformations,

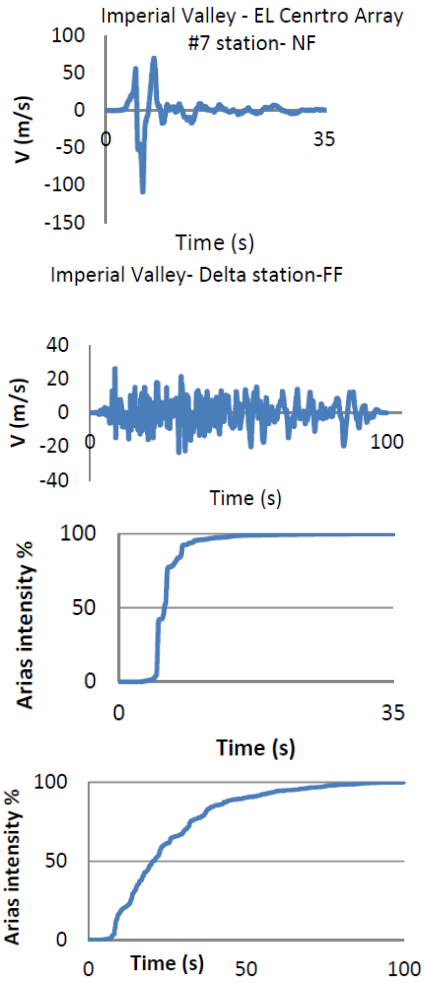

Fig. 6 Time history of earthquake velocity and Arias intensity for sample NF and FF ground motions

Table 4 FF and NF ground motion sets used in the NLTHA

	Event name	Year	Record length (s)	Station	PGA (g)	M	Site source distance(km)
Near-Fault record	Imperial valley-06	1979	39	El centro Array#6	0.44	6.5	27.5
	Imperial valley-06	1979	37	El centro Array#7	0.46	6.5	27.6
	Irpinia. Italy-01	1980	40	Sturno	0.31	6.9	30.4
	Superstition-hills-02	1987	22.3	Parachute test site	0.42	6.5	16
	Loma Prieta	1989	40	Saratoga-Aloha	0.38	6.9	27.2
	Erizican-Turkey	1992	20.8	Erizican	0.49	6.7	9
	Cape Mendocino	1992	36	Petrolia	0.63	7	4.5
	Landers	1992	48	Lucerne	0.79	7.3	44
	Northridge-01	1994	20	Rinaldi Receiving Sta	0.87	6.7	10.9
	Northridge-01	1994	40	Sylmar-Olive View	0.73	6.7	16.8
	Kocaeli/IZT	1999	30	Izmit	0.22	7.5	5.3
	Chi chi, Taiwan	1999	90	TCU065	0.82	7.6	26.7
	Chi chi, Taiwan	1999	90	TCU102	0.29	7.6	45.6
	Duzce	1999	26	Duzce	0.52	7.1	1.6
Far-Fault record	Northridge	1994	20	Canyon Country-WLC	0.48	6.7	26.5
	Duzce	1999	56	Bolu	0.82	7.1	41.3
	Hector Mine	1999	45.3	Hector	0.34	7.1	26.5
	Imperial valley	1979	100	Delta	0.35	6.5	33.7
	Imperial valley	1979	39	El centro Array#11	0.38	6.5	29.4
	Kobe, Japan	1995	41	Shin- Osaka	0.24	6.9	46
	Kocaeli, Turkey	1999	27.2	Duzce	0.36	7.5	98.2
	Kocaeli, Turkey	1999	30	Arcelik	0.22	7.5	53.7
	Landers	1992	44	Yermo Fire Station	0.24	7.3	86
	Loma Prieta	1989	40	Gilroy Array	0.56	6.9	31.4
	Superstition Hills	1987	40	El Centro lmp. Co.	0.36	6.5	35.8
	Superstition Hills	1987	22.3	Poe Road (temp)	0.45	6.5	11.2
	Chi chi, Taiwan	1999	90	Chy101	0.44	7.6	32
	San Fernando	1971	28	LA-Hollywood Stor	0.21	6.6	39.5

the motion pulses are usually reported perpendicular to the active causative fault. The pulses are commonly reported in the velocity time history of fault-normal components (Somerville 1997). For instance, Fig. 6 shows the velocity time histories and Arias intensity (I_a) corresponding to one NF and one FF record. The Arias intensity (Arias 1970) is a measure of the energy content of an earthquake record associated with event duration. I_a is defined as Eq. (2) and is believed to be a rational indicator of potential earthquake destructiveness

$$I_a = \frac{\pi}{2g}\int_0^{t_f} (a(t))^2\, dt \tag{2}$$

Where g is gravity acceleration, t_f is total duration of ground motion, and $a(t)$ is the time history of ground acceleration. I_a in the NF event has a quick rising that happens coincident with velocity pulse occurrence. The NF ground motions are usually rich in high frequencies and sometimes contain fling-step effects. Among the NF record characteristics that are directivity pulses, high frequency content and fling-step, the first one is the most important in structural engineering in relation to the NF topic.

A set of 14 horizontal near-fault pulse-like and 14 ordinary far-fault earthquake records was selected from the ground motions given in Tables A-6A and Table A-4A of the FEMA P695 (2009), respectively. The time histories of the events were obtained from PEER NGA data base. Only fault normal components of the ground motions were used in the analysis. All seismic records are summarized in Table 4.

According to LATBSDC, the maximum considered earthquake (MCE) level was used to scale the records (LATBSDC 2014). The scaling method to prepare suitable acceleration time history is essential for dynamic analysis (Beiraghi *et al.* 2016c). It is assumed that the spectrum curve for MCE level was 1.5-times the response spectrum curve in DBE level (ASCE 7 2010). Record scaling was carried out such that the average value of the 5% damped spectrum graph for periods ranging from 0.2T to 1.5T was located above the MCE spectrum, where T is the first mode period of the natural vibration (ASCE 7 2010). The average of scaled spectra for the near-fault and far-fault records is illustrated in Fig. 7.

3.5 Damping modeling

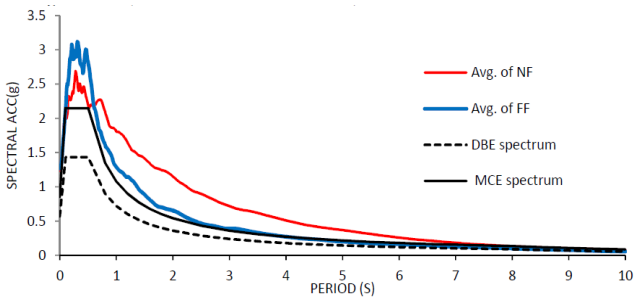

Fig. 7 MCE, DBE, mean NF and mean FF acceleration response spectra

The damping coefficient quantity is known to severely affect the behavior of a structure subjected to NLTHA (Priestley *et al.* 2005). Perform-3D software is capable to implement Rayleigh damping and modal damping. The software user guide recommends the use of a combination of modal and Rayleigh damping (Perform-3D User Guide 2006). In this study, in addition to modal damping, a small amount of Rayleigh damping was used to damp out high-frequency vibrations. To use the Rayleigh damping, two modes must be selected. It is common to select the first mode and the mode for which accumulated modal mass participation is bigger than 90% of the total mass. In this study, 2.5% of the modal damping for all modes alongside 0.15% Rayleigh damping for the first and third modes were used as recommended by the software guidelines (Perform-3D User Guide 2006).

4. Energy equations

Two procedures have been proposed for calculating the earthquake input energy according to Uang and Bertero (1990): one is based on the absolute displacement and the other is based on relative displacement. The main difference between the two procedures is the less importance of damage evaluation, since the inelastic energy which is related to the damage potential of structures, is not dependent on the type of approach used (Khashaee *et al.* 2003). According to Chopra (2001), Bruneau and Wang (1996), since internal forces within a structure are computed based on relative displacements and velocities, the input energy should be calculated in terms of the relative displacement (Khashaee *et al.* 2003). Therefore, the calculation of energy based on the relative displacement was used in this paper.

The equation of motion for a structure with N degrees of freedom can be written as

$$F_i(t) + F_d(t) + F_s(t) = -Mr\ddot{u}_g(t) \tag{3}$$

where F_i is an N-dimensional inertia force vector, F_d is an N-dimensional damping force vector, F_s is an N-dimensional non-linear stiffness force vector, M is the mass matrix, r is an N-dimensional influence vector, and $\ddot{u}_g$ denotes ground acceleration.

During earthquake, depending on the site specifications, structure specifications, and the strong ground motion specifications like frequency contents of the records, the structures receive different amounts of earthquake energy. Due to the transferred energy to the structure by the severe events, the responses in the structure lead to elastic and inelastic deformations in the structural elements.

The Eq. (3) is transposed and is then multiplied by $du = \dot{u}dt$ on both sides. By integrating, the energy balance equation is obtained

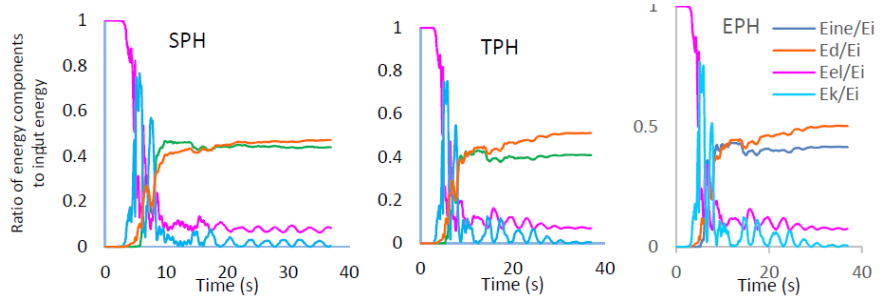

(a) Imperial Valley - EL Cenrtro Array #7 station

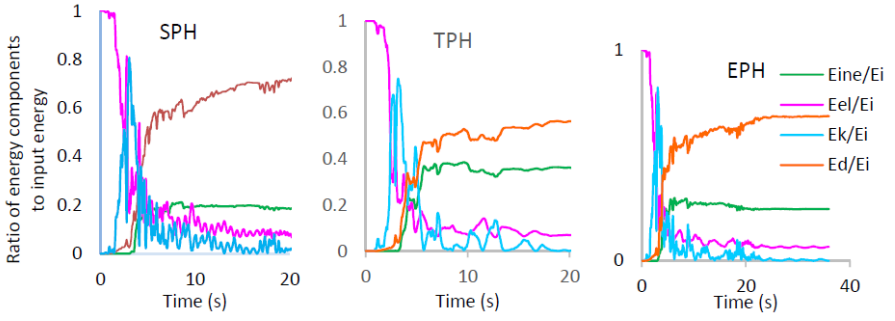

(b) Cape Mendocino - Petrolia station

Fig. 8 Time history of E_{ine}/E_i, E_d/E_i, E_k/E_i and E_{el}/E_i for the 50-story building subjected to sample NF records

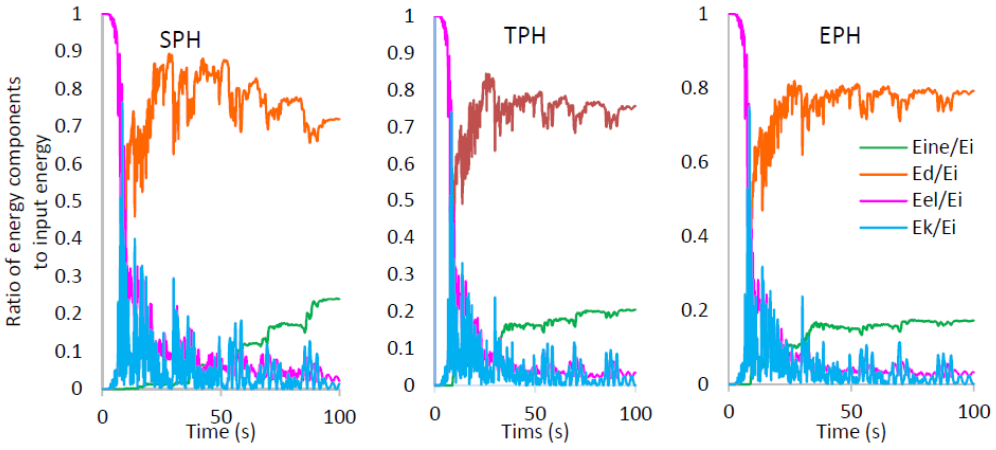

(a) Imperial Valley- Delta station

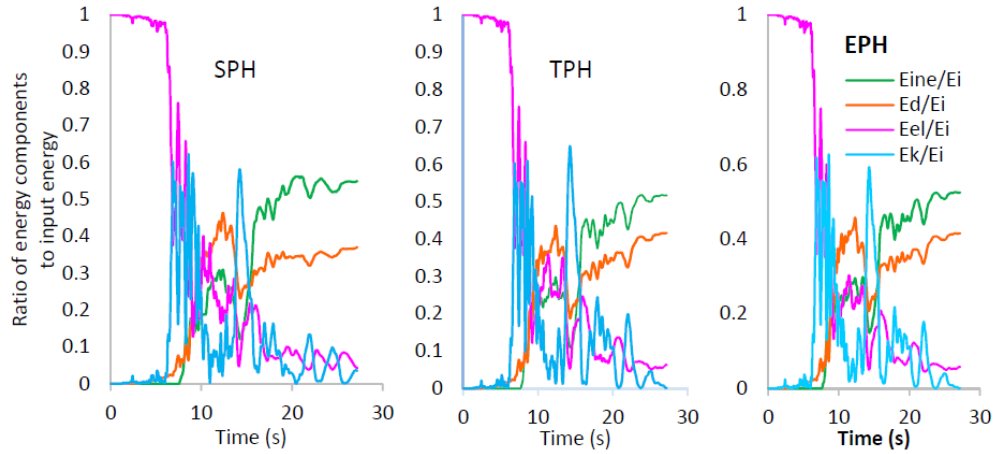

(b) Kocaeli, Turkey- Duzce station

Fig. 9 Time history of E_{ine}/E_i, E_d/E_i, E_k/E_i and E_{el}/E_i for the 50-story building subjected to sample FF records

$$\int_0^u F_i^T(t)\,du + \int_0^u F_d^T(t)du + \int_0^u F_s^T(t)\,du = -\int_0^u M\,r\ddot{u}_g(t)du \tag{4}$$

Where u is an N-dimensional relative displacement vector. From left, the first term is the kinetic energy corresponding to the masses E_k, the second term is the energy dissipated by the damping E_d, and the third term is the internal work or energy absorbed by the structural members that comprises elastic E_{el} and inelastic (hysteresis) energy, E_{ine}. Structural damage occurs when the deformations enter the inelastic range. The right term is the total relative input energy E_i.

Eq. (5) summarizes the energy equilibrium equation described earlier. This equation shows that the input energy imposed on the structure by the earthquake is equal to the other four energies related to the structural properties at any time.

$$E_k + E_d + (E_{el} + E_{ine}) = E_i \tag{5}$$

5. Dynamic analysis and results

NLTH analysis was performed using NF and FF earthquake records. Values of various types of the energies mentioned in the previous part were calculated. Figs. 8 and 9 show the values of different kinds of energy in the 50-storey structure during an earthquake for two NF and two FF events, respectively. Records of Delta station from Imperial Valley earthquake as well as the Duzce station from Kocaeli earthquake were selected as sample FF events. Also, records of El Centro Array #7 station from Imperial Valley-06 earthquake as well as the Petrolia station from Cape Mendocino earthquake were selected as NF event examples. In these diagrams, the horizontal axis represents time. In the vertical axis, the values of energy are divided by E_i value. Energy responses pertaining to the E_{ine}/E_i, E_k/E_i, E_d/E_i and E_{el}/E_i are depicted separately for SPH, TPH and EPH approaches. It is obvious that in the early time of oscillation, when the structure is in range of linear response, the E_{el}/E_i and E_k/E_i ratios are relatively large values and during the ground motion by reducing the contribution of one of them, the other one increases and vice versa. The logic of this phenomenon is similar to what is described in the references of structure dynamic for elastic systems vibration.

When the structure experiences nonlinear deformations, the values of E_{el}/E_i and E_k/E_i reduce greatly, because a

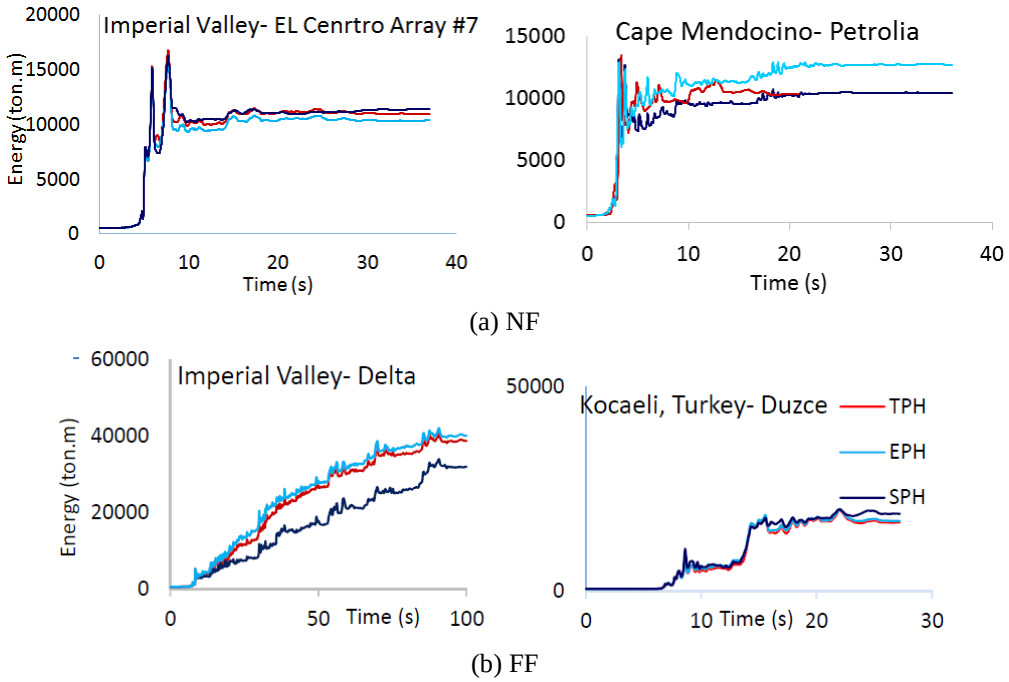

(a) NF

(b) FF

Fig. 10 Total input energy for the SPH, TPH and EPH approaches during the sample events for the 50-story building

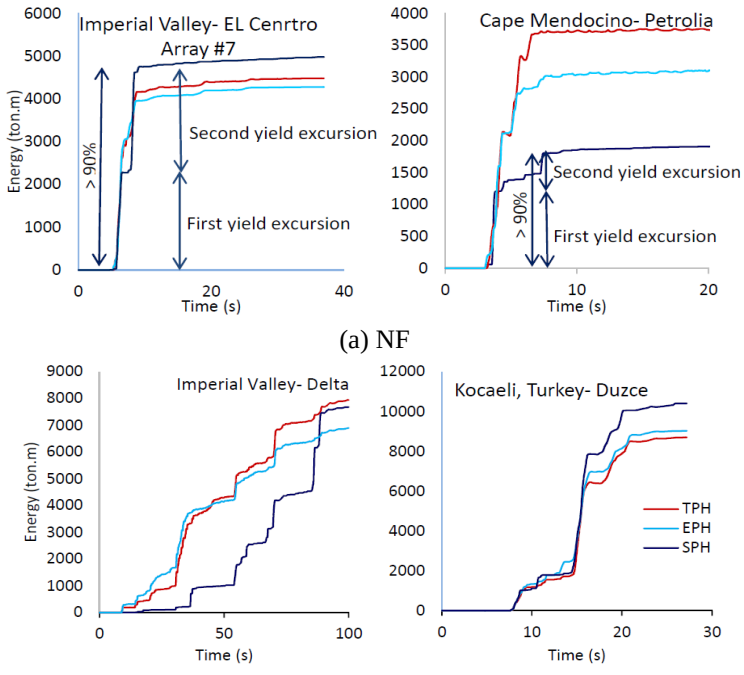

(a) NF

(b) FF

Fig. 11 Accumulated inelastic energy for the SPH, TPH and EPH approaches during the sample events for the 50-story building

significant portion of the input energy is changed to two other types of energy, including inelastic energy and damping energy.

Fig. 10 compares the input energy demand from the SPH, TPH and EPH approaches pertaining to a 50-storey structure for two cases of NF and FF earthquakes. As observed, it cannot be principally concluded that an approach like SPH, in all earthquakes has the lowest or highest energy input at the end of earthquake's duration. This is due to differences in frequency content and differences in other characteristics of earthquake records. In NF earthquakes, the maximum input energy demand occurs with the arriving velocity pulse to structure simultaneously. This fact is revealed by comparing the pulse arrival time in velocity time history (Fig. 5) and rising time of E_i diagram's value. But, the FF events lack velocity pulse and thus, unlike the NF events, do not have severe sudden rising in the E_i diagram. In FF events, the values of E_i increase with

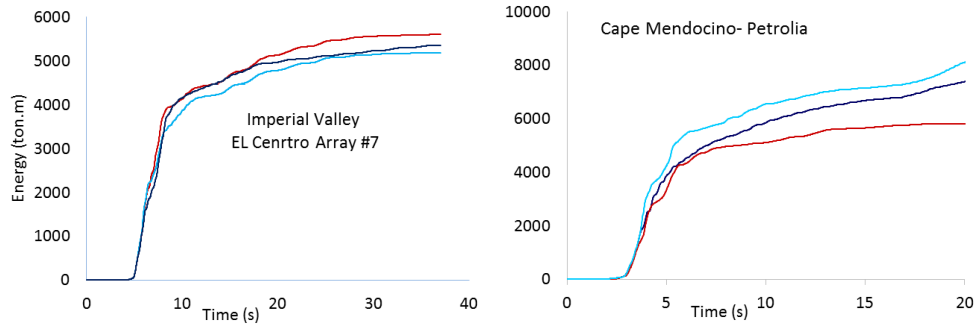

(a) NF

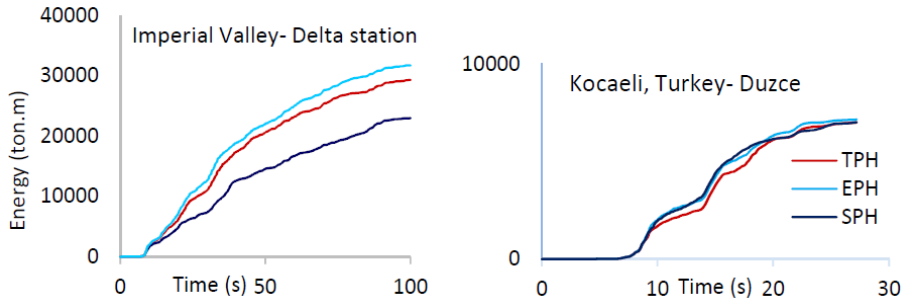

(b) FF

Fig. 12 Accumulated damping energy for the SPH, TPH and EPH approaches during the sample events for the 50-story building

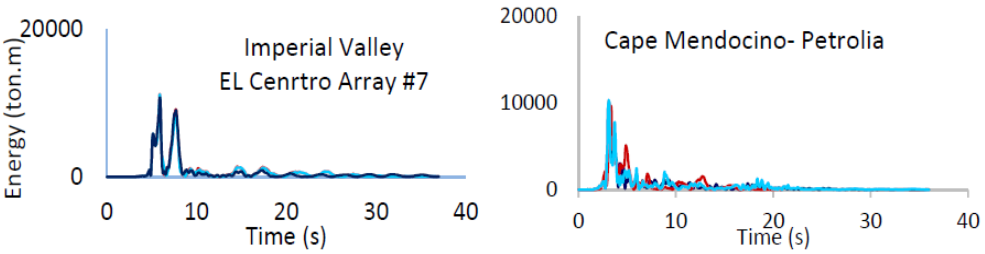

(a) NF

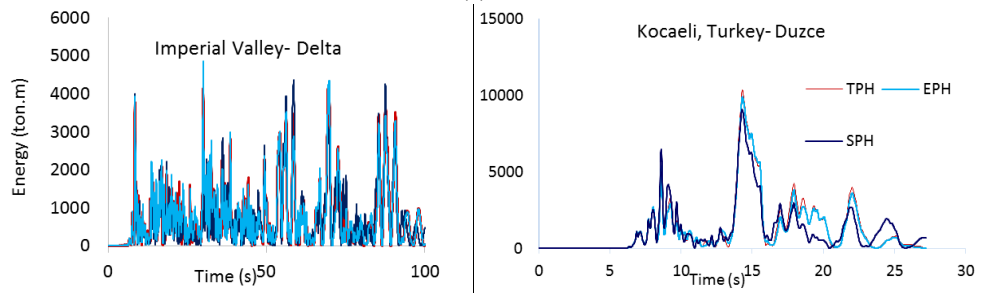

(b) FF

Fig. 13 Time history of kinetic energy for the SPH, TPH and EPH approaches during the sample events for the 50-story building

a relatively mild trend. The maximum amount of input energy in FF earthquake occurs at end times of earthquake, whereas in NF earthquakes this maximum amount coincides with the arrival of velocity pulse to structure in early times of earthquake record. It should be noted that the occurrence of maximum input energy demand during the initial times of motion is only true for records in which velocity pulse is resulted from acceleration pulse integral and this phenomenon is not observed in records whose velocity pulse results from succession of high acceleration peaks (and have no acceleration pulse) (Kalkan and Kunnath, 2006)

For NF earthquakes, Fig. 10 shows that SPH approach at the end of one earthquake record has the least E_i demand, while for the other earthquake record, it has the highest E_i demand. The comparison of diagrams in Fig. 10 shows that time history of energy demand in each structure is associated not only with the characteristics of earthquake but also with structural specifications.

Essentially, the failure potential of a structure depends

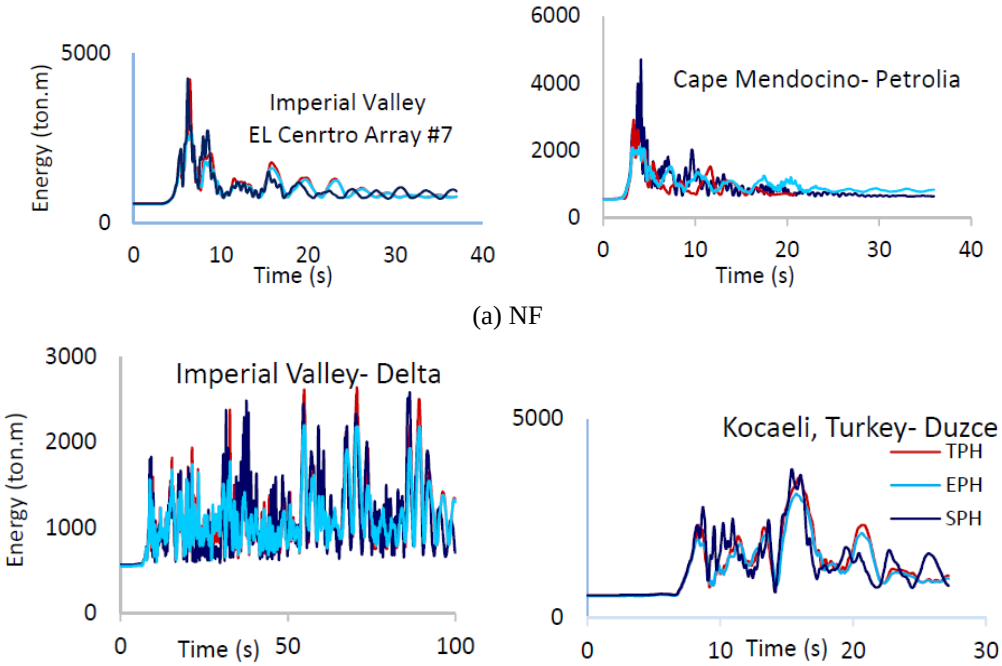

Fig. 14 Time history of elastic strain energy for the SPH, TPH and EPH approaches during the sample events for the 50-story building

on the maximum inelastic energy demand during an earthquake. Inelastic energy absorbed by the structure during the earthquake for the two NF and the two FF sample earthquakes in the 50-storey structure is shown in Fig. 11. For an individual record, there is not a general rule to determine which approach, among SPH, TPH and EPH, has the lowest or the highest amount of inelastic energy demand. Again, inelastic energy demand in each approach pertaining to each individual earthquake, is associated not only with characteristics of earthquake but also with structural specifications. However, on average, it will be demonstrated that the inelastic energy has a regular trend for all the NF and FF records. Also, the maximum amount of inelastic energy occurs at the end time of earthquake. The reason is that values of inelastic energy diagram are cumulative. Remarkably, a sudden increase in inelastic energy demand under the NF events generally occurs in two absolute steps simultaneous with the arrival of earthquake pulse to structure that reflects damage potential.

In this study, the average time during which 90% of inelastic energy of FF earthquakes is absorbed by structure is about four times the time during which the same amount of inelastic energy of NF earthquake is absorbed by structure. The Fig. shows that more than 90% of inelastic energy demand appears during the first yield excursion or during the first and the second yield excursion. The high energy applied in a very short time will intensify the structural damage.

Time histories of damping energy demands during the earthquake in 50-storey structure under the selected NF and FF earthquake are shown in Fig. 12. The least damping energy under the FF earthquake belongs to the SPH approach, but it should be noted that this is not generalizable to all records**.** Since damping energy depends mainly on the system velocity, in NF earthquakes, coinciding with the arrival of velocity pulse to structure, the increase of the diagram value with a relatively strong rate occurs. This phenomenon is not observed in the FF earthquakes.

Fig. 13 illustrates diagrams pertaining to kinetic energy demand for a 50-storey structure subjected to the NF and FF earthquakes. It is obvious that in NF events, simultaneous with the arrival of velocity pulse to structure, significant amounts of kinetic energy are imposed on structure. But, this phenomenon does not occur under the FF events. In general, for an assumed event, the overall values of kinetic energy demand curves pertaining to SPH, TPH and EPH approaches, do not show any considerable difference. This is due to the insignificant differences among stories velocity in SPH, TPH and EPH approaches subjected to identical earthquakes. It should be noted that according to the equation presented for calculating kinetic energy, the amount of kinetic energy is just a function of velocity and mass of stories.

Time history responses of the elastic energy demand of a 50-storey structure for SPH, TPH and EPH approaches under different earthquakes are shown in Fig. 14. As mentioned in the case of kinetic energy, due to the presence of pulse in NF events, simultaneous with arrival of pulse at the early time of earthquakes, elastic energy demand increases relatively and suddenly. But immediately after the occurrence of nonlinear deformations in structure, Eel value has a significant decrease in a short time and then continues downward with a slight slope. Also, the diagrams of elastic energy demand for all three approaches under considered earthquakes are almost the same, since the displacement

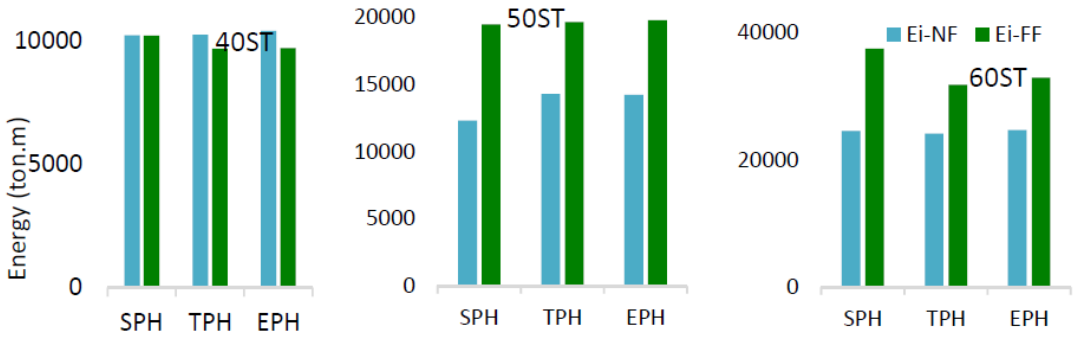

Fig. 15 Comparison of NF and FF record effect on average total input energy demand at the end of earthquake durations

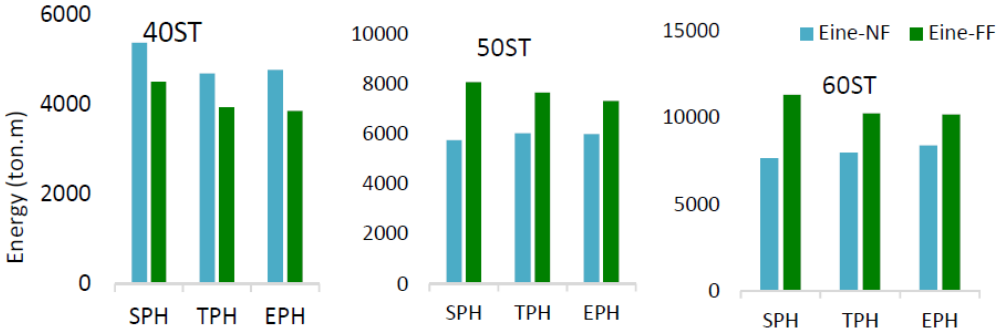

Fig. 16 Comparison of NF and FF record effect on average inelastic energy at the end of earthquake durations

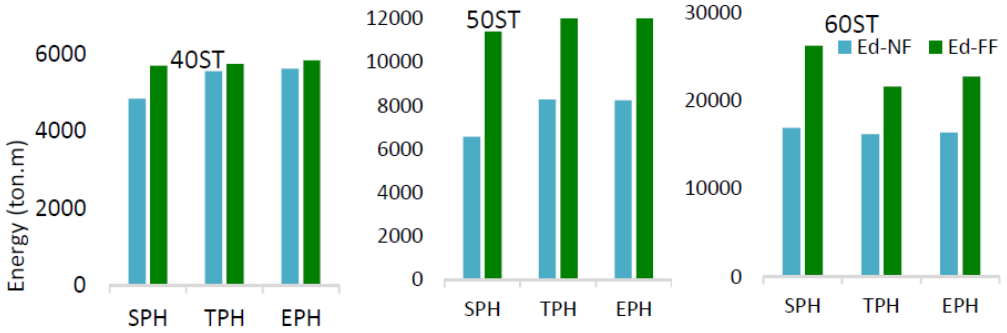

Fig. 17 Comparison of NF and FF record effect on average damping energy at the end of earthquake durations

demand and elastic stiffness of a structure's stories in different approaches under a given earthquake are almost identical.

The comparison between NF and FF records effect pertaining to average total energy, resulting from the sum of damping energy and inelastic energy at the end of structure vibration, is shown in Fig. 15. In 50- and 60-storey structures, the average value of total input energy resulting from all NF earthquakes in all three approaches (SPH, TPH and EPH) is less than the corresponding average value under all FF earthquakes. This is reversed in 40-storey structure. Also, the Fig. shows that for each set of NF or FF records, the difference in the average value of the total input energy at the end of vibration for each SPH, TPH and EPH approaches is not very noticeable.

Fig. 16 compares average inelastic energy demand at the end of structures vibration under all NF and FF records. It is obvious that in 40-storey structure, average inelastic energy demand obtained by the NF earthquake in all three approaches (SPH, TPH and EPH) was approximately 1.15 times the corresponding value from FF earthquakes. This phenomenon was reversed in 50 and 60-storey structures in such a way that the mentioned ratio for these structures is 0.77 and 0.76, respectively. Thus, in higher structures, FF earthquakes imposed more overall inelastic energy demand compared with NF earthquakes.

Average values of damped energy subjected to all NF and FF earthquakes at the end of structure vibration are compared in Fig. 17. Generally, in all three approaches (SPH, TPH and EPH), the average value of damping energy resulting from the NF earthquake is less than the corresponding value resulting from FF earthquake and this issue is more evident for higher structures. Comparison between NF and FF records effect pertaining to average inelastic energy demand in the core-wall along the height for EPH approach is illustrated in Fig. 18. The vertical axis represents normalized height of the structure and the horizontal axis shows value(s) of equivalent velocity (Ve) related to energy (E) and seismic mass (M) that can be obtained from the following equation

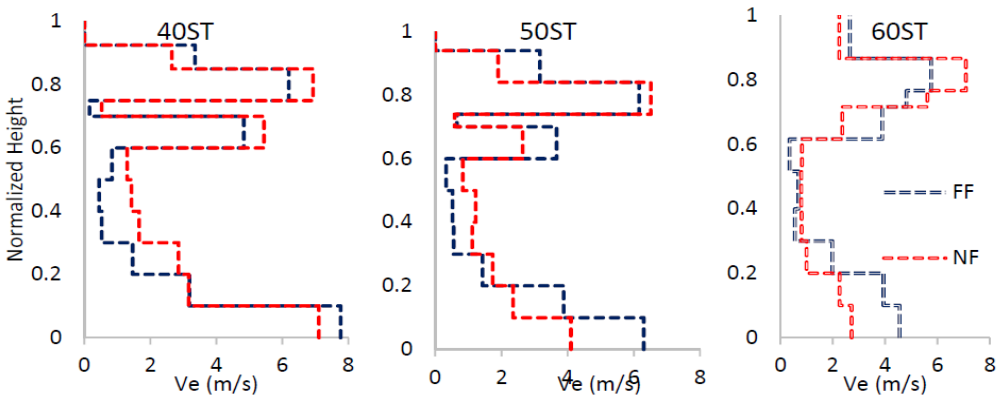

Fig. 18 Average inelastic energy distribution pattern along the height of the EPH models for NF and FF events

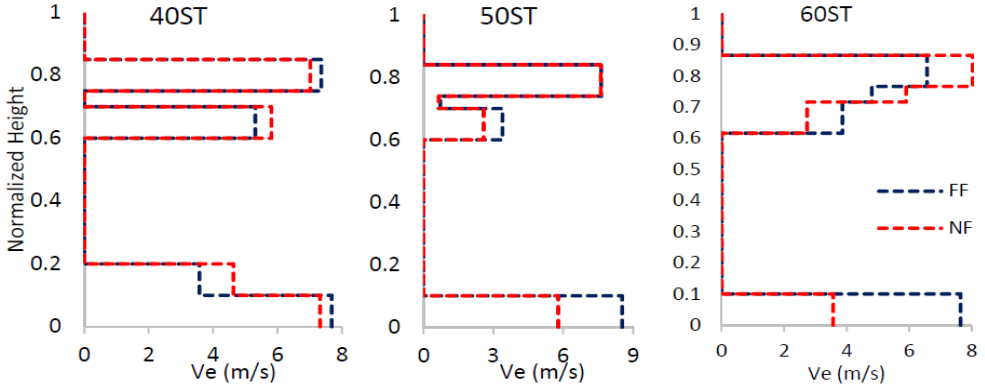

Fig. 19 Average inelastic energy distribution pattern along the height of the TPH models for NF and FF events

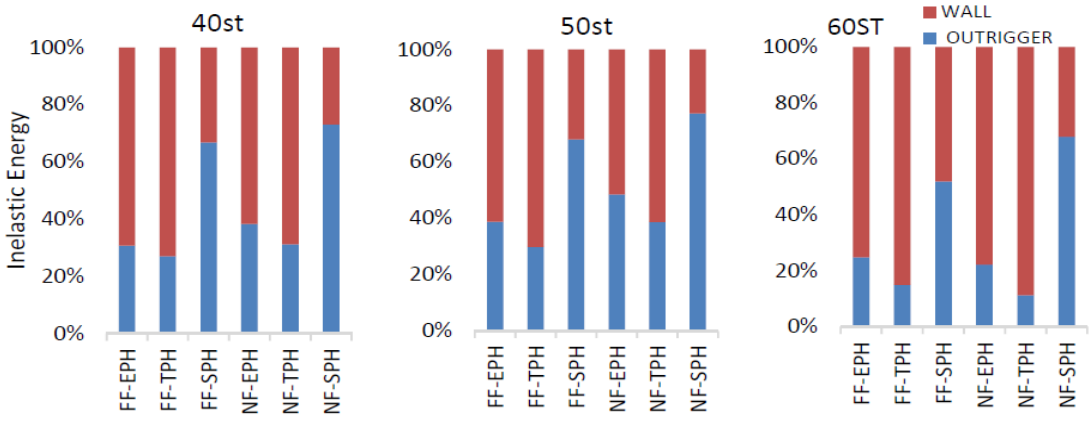

Fig. 20 Contribution of outrigger and core-wall in the average inelastic energy demand for different approaches subjected to NF and FF events

$$V_e = \sqrt{\frac{2E}{M}} \tag{6}$$

With respect to the distribution of average inelastic core-wall energy demand, it is found that principally at the base of core-wall as well as adjacent to above and below of outrigger level, more inelastic energy values are absorbed due to large moment demand resulting from earthquake load. Also, in general, FF earthquakes at the base of core-wall cause larger mean inelastic energy demand compared with NF earthquakes. While NF earthquakes create larger inelastic energy demand in adjacent outrigger level on the wall compared to FF earthquakes. The difference between average inelastic energy demand pertaining to the NF and FF records is more noticeable for taller buildings.

Fig. 19 compares the same items in above paragraph for the TPH approach. The general trend of diagrams is consistent with what stated for EPH approach. It should be noted that in the 60-storey structure, the average inelastic energy demand in base level of core-wall under FF earthquakes is about 1.7 times the corresponding value under NF earthquakes.

Fig. 20 shows the contribution of core-wall and outrigger in inelastic energy absorbed by the studied models. On average for the total NF and FF events, in the SPH approach, it is obvious that more than 65 percent of inelastic energy, is absorbed by BRBs in outrigger. While in TPH and EPH approaches, outrigger contribution in inelastic energy demand is reduced. It should be noted that the contribution of outrigger in inelastic energy absorption for the TPH and EPH approaches does not show significant difference in such a way that the mentioned value is approximately 25 and 30 percent, respectively. One reason for this phenomenon is that in SPH approach only 10 percent of the wall height is involved in energy dissipation and 90 percent of wall above the base plastic hinge remains elastic. Another reason is that in higher levels of SPH model only outrigger is involved for absorbing inelastic energy. In fact, in the TPH and EPH approaches, wall participation in energy absorption in higher levels would reduce the share of outrigger in inelastic energy absorption.

6. Conclusions

In this study, various energy demands for the 40-, 50- and 50-story cantilever RC core-wall connected to BRB outriggers with SPH, TPH and EPH approaches for core-wall were investigated. To create the numerical wall model, nonlinear fiber elements were used. The forward directivity near-fault and ordinary far-fault records were used for nonlinear dynamic analysis. In terms of energy demand, the following results were deduced:

- The time during which 90% of the input inelastic energy occurs subjected to the FF records was 4 times larger than the time during which the same input inelastic energy occurs subjected to the NF records.
- The time-history ratio of the kinetic and elastic strain energy demands to input energy (E_k/E_i,E_{el}/E_i) showed large oscillations in the linear portion of structure vibration at the early time of earthquake and this was more severe with the NF earthquakes. These oscillations disappeared rapidly as the structures experienced nonlinear deformation because a significant portion of the input energy was distributed among inelastic and damping energies rather than the kinetic and elastic strain energies.
- In 40-storey structure, average total inelastic energy demand for all three approaches obtained from the NF earthquakes at the end of structure vibration was 1.15 times the corresponding value obtained from FF earthquakes. This phenomenon was reversed in 50 and 60-storey structures in such a way that the mentioned ratio is 0.77 and 0.76, respectively. Thus, in higher structures, FF earthquakes imposed more overall inelastic energy demand compared with NF earthquakes.
- In the EPH approaches, with respect to the distribution of average inelastic energy demand along the height of core-wall, principally most average inelastic energies at the base of core-wall as well as adjacent to above and below of outrigger level, are absorbed due to large moment demand in these regions of core-wall resulting from earthquake load.
- In general, for both EPH and TPH approach, FF earthquakes at the base of core-wall cause a larger average inelastic energy demand compared with NF earthquake. While NF earthquakes create larger average inelastic energy demand in adjacent outrigger level on the core-wall compared to FF earthquakes.
- On average, for all NF and FF events, in the SPH approach, more than 65 percent of inelastic energy is absorbed by BRBs in outrigger. While in TPH and EPH approaches, outrigger contribution in inelastic energy demand is reduced. It should be noted that the contribution of outrigger in inelastic energy absorption for the TPH and EPH approaches does not show a significant difference in such a way that the mentioned value is approximately 25 and 30 percent, respectively. One reason for this phenomenon is that in SPH approach only 10 percent of the wall height is involved in energy dissipation and 90 percent of wall above the base plastic hinge remains elastic. Another reason is that in higher levels of SPH model only outrigger is involved in absorbing inelastic energy.

References

ACI 318-14 (2014), Building code requirements for structural concrete and commentary, ACI Committee 318, Farmington Hills.

AISC (2005), Seismic Provision for structural steel buildings. American Institute of Steel Construction, Chicago.

Applied Technology Council (2010), ATC-72: Modeling and Acceptance Criteria for Seismic Design and Analysis of Tall Buildings, ATC, Redwood City, CA.

Arias, A. (1970), *A Measure of Earthquake Intensity*, Ed. R.J. Hansen, *Seismic Design for Nuclear Power Plants*, MIT Press, Cambridge, Massachusetts.

Bobby, S., Spence, S. M., Bernardini, E. and Kareem, A. (2014), "Performance-based topology optimization for wind-excited tall buildings: a framework", *Eng. Struct.*, **74**, 242-255.

Bosco, M. and Marino, E.M. (2013), "Design method and behavior factor for steel frames with buckling restrained braces", *Earthq. Eng. Struct. Dyn.*, **42**, 1243-1263.

Beiraghi, H., Kheyroddin, A. and Kafi, M.A. (2015), "Nonlinear fiber element analysis of a reinforced concrete shear wall subjected to earthquake records", *Tran. Civil Eng.*, **39**, 409-422.

Beiraghi, H., Kheyroddin, A. and Kafi, M.A. (2016a), "Forward directivity near-fault and far-fault ground motion effects on the behavior of reinforced concrete wall tall buildings with one and more plastic hinges", *Struct. Des. Tall Spec. Build.*, **25**(11), 519-539.

Beiraghi, H. and Siahpolo, N. (2017), "Seismic assessment of RC core-wall building capable of three plastic hinges with outrigger", *Struct. Des. Tall Spec. Build.*, **26**, e1306

Beiraghi, H., Kheyroddin, A. and Kafi, M.A. (2016b), "Energy dissipation of tall core-wall structures with multi-plastic hinges subjected to forward directivity near-fault and far-fault earthquakes", *Struct. Des. Tall Spec. Build.*, **25**, 801-820.

Beiraghi, H., Kheyroddin, A. and Kafi, M.A. (2016c), "Effect of record scaling on the behavior of reinforced concrete core-wall buildings subjected to near-fault and far-fault earthquakes", *Scientia Iranica. Tran. A Civil Eng.*, **24**(3), 884.

Bruneau, M. and Wang, N. (1996), "Some aspects of energy methods for the inelastic seismic response of ductile SDOF

structures", *Eng. Struct*., **18**(1), 1-12.
Chopra, A.K. (2001), *Dynamics of Structures*, Prentice-Hall, New Jersey.
Chen, Y., McFarland, D.M., Wang, Z., Spencer Jr, B.F. and Bergman, L.A. (2010), "Analysis of tall buildings with damped outriggers", *J. Struct. Eng*., **136**(11), 1435-1443.
Calugaru, V. and Panagiotou, M. (2012), "Response of tall cantilever wall buildings to strong pulse type seismic excitation", *Earthq. Eng. Struct. Dyn*., **41**, 1301-1318
Eskandari, R. and Vafaei, D. (2015), "Effects of near-fault records characteristics on seismic performance of eccentrically braced frames", *Struct. Eng. Mech*., **56**(5), 855-870.
Eskandari, R., Vafaei, D., Vafaei, J. and Shemshadian, M.E. (2017), "Nonlinear static and dynamic behavior of reinforced concrete steel-braced frames", *Earthq. Struct.*, **12**(2), 191-200.
Fajfar, P. (1992), "Equivalent ductility factors, taking into account low-cycle fatigue", *Earthq. Eng. Struct. Dyn*., **23**, 507-21.
Fanaie, N. and Afsar Dizaj, E. (2014), "Response modification factor of the frames braced with reduced yielding segment BRB", *Struct. Eng. Mech*., **50**(1), 1-17.
Esmaili, O., Epackachi, S., Mirghaderi, R., Taheri Behbahani, A.A. and Vahdani, S. (2011), "Rehabilitation of a high-rise coupled shear wall system in a 56-storey residential reinforced concrete building (Tehran Tower), based on nonlinear dynamic time-history analyses", *Struct. Des. Tall Spec. Build*., **20**(8), 1035-1047.
FEMA P695 (2009), Quantification of Building Seismic Performance Factors (ATC-63 Project), Federal Emergency Management Agency, Washington D.C.
Mander, J.B., Priestley, M.J.N. and Park, R. (1988), "Theoretical Stress-Strain Model for Confined Concrete", *ASCE J. Struct. Eng*., **114**(8), 1804-1826
Ghorbanirenani. I., Tremblay, R., Léger, P. and Leclerc, M. (2012), "Shake table testing of slender rc shear walls subjected to eastern north america seismic ground motions", *J. Struct. Eng*., **138**(12), 1515-1529.
Ghodsi, T., Ruiz, J.F., Massie, C. and Chen, Y. (2010), Pacific earthquake engineering research/seismic safety commission tall building design case study", *Struct. Des. Tall Spec. Build*., **19**(2), 197-256.
Haselton, C.B., Liel, A.B., Deierlein, G.G., Dean, B.S. and Chou, J.H. (2011), "Seismic collapse safety of reinforced concrete buildings: I. assessment of ductile moment frames", *J. Struct. Eng*., **137**(4), 481-491.
Hall, J.F., Heaton, T.H., Halling, M.W. and Wald, D.J. (1995), "Near-source ground motion and its effects on flexible buildings", *Earthq. Spectra*., **11**, 569-605.
Housner, G.W. (1956), "Limit design of structures to resist earthquakes", *Proceedings of 1st World Conference on Earthquake Engineering*, Earthquake Engineering Research Institute, Oakland, Calif, USA.
Iervolino, I. and Cornell, C.A. (2008), "Probability of occurrence of velocity pulses in near-source ground motions", *Bull. Seismol. Soc. Am*., **98**(5), 2262-2277.
Jones, P. and Zareian, F. (2009), "Seismic response of a 40-storey buckling-restrained braced frame designed for the Los Angeles region", *Struct. Des. Tall Spec. Build*., **22**(3), 291-299.
Marzban, S., Banazadeh, M. and Azarbakht, A. (2014), "Seismic performance of reinforced concrete shear wall frames considering soil-foundation-structure interaction", *Struct. Des. Tall Spec. Build*., **23**(4), 302-318.
Massumi, A. and Monavari, B. (2013), "Energy based procedure to obtain target displacement of reinforced concrete structures", *Struct. Eng. Mech*., **48**(5), 681-695
Kalkan, E. and Kunnath, S.K. (2006), "Effects of fling-step and forward directivity on the seismic response of buildings", *Earthq. Spectra*., **22**(2), 367-390.
Khashaee, P., Mohraz, B., Sadek, F., Lew, H.S. and Gross, J.L. (2003), "Distribution of earthquake input energy in structures", Report no. NISTIR 6903, Building and Fire Research Laboratory, National Institute of Standards and Technology, Gaithersburg.
Klemencic, R., Fry, A., Hooper, J.D. and Morgen, B.G. (2007), "Performance based design of ductile concrete core wall buildings-issues to consider before detail analysis", *Struct. Des. Tall Spec. Build*., **16**, 599-614.
Kuwamura, H. and Galambos, T.V. (1989), "Earthquake load for structural reliability", *J. Struct. Eng*., ASCE, **115**(6), 1446-1462.
LATBSDC (2011), An Alternative Procedure For Seismic Analysis and Design of Tall Buildings Located in the Los Angeles Region, Los Angeles Tall Buildings Structural Design Council.
Liel, A.B., Haselton, C.B. and Deierlein, G.G. (2011), "Seismic collapse safety of reinforced concrete buildings: II. comparative assessment of non-ductile and ductile moment frames", *J. Struct. Eng*., **137**(4), 492-502.
Luco, N. and Cornell, A. (2007), "Structure-specific scalar intensity measures for near source and ordinary earthquake ground motions", *Earthq. Spectra*, **23**(2), 357-92.
Mortezaei, A. and Ronagh, H.R. (2013), "Plastic hinge length of reinforced concrete columns subjected to both far-fault and near-fault ground motions having forward directivity", *Struct. Des. Tall Spec. Build*., **22**(12), 903-926.
National Institute of Standards and Technology (2012), Seismic Design of Cast-in-Place Concrete Special Structural Walls and Coupling Beams, NEHRP Seismic Design Technical Brief No. 6.
Nguyen, A.H., Chintanapakdee, C. and Hayashikawa, T. (2011), "Assessment of current nonlinear static procedures for seismic evaluation of BRBF buildings", *J. Constr. Steel Res*., **66**(8-9), 1118-1127.
Orakcal, K. and Wallace, J. (2006), "Flexural modeling of reinforced concrete walls-experimental verification", *ACI Struct. J*., **103**(2), 196-206.
Powell, G. (2007), *Detailed Example of a Tall Shear Wall Building using CSI's Perform 3D Nonlinear Dynamic Analysis*, Computers and Structures Inc. Berkeley, CA.
Panagiotou, M. and Restrepo, J. (2009), "Dual-plastic hinge design concept for reducing higher-mode effects on high-rise cantilever wall buildings", *Earthq. Eng. Struct. Dyn.*, **38**, 1359-1380.
PERFORM-3D (2011), Nonlinear Analysis and Performance Assessment for 3D Structures, V.4.0.3, Computers and Structures, Inc., Berkeley, CA.
PERFORM-3D (2006), Nonlinear Analysis and Performance Assessment for 3D Structures, V.4, User Guide, Computers and Structures, Inc., Berkeley, CA.
Priestley, M.J.N. and Grant, D.N. (2005), "Viscous damping in seismic design and analysis", *J. Earthq. Eng.*, **9**(SP2), 229-255.
Paulay, T. and Priestley, M.J.N. (1992), *Seismic Design of Reinforced Concrete and Masonry Buildings*, Wiley, Hoboken, NJ.
Riddell, R. and Garcia, E.J. (2001), "Hysteretic energy spectrum and damage control", *Earthq. Eng. Struct. Dyn.*, **30**, 1791-1816.
Rahgozar, R. and Sharifi, Y. (2009), "An approximate analysis of Framed tube, Shear core and Belt truss in high-rise building", *Struct. Des. Tall Spec. Build*., **18**, 607-624.
Simpson, Gumpertz, & Heger, Inc. (2009), Detailed Design Write up for BRBF building, Simpson, Gumpertz, & Heger, Inc., San Francisco, CA.
Somerville, P. (1997), "The characteristics and quantification of near-fault ground motion", *Proceedings of the FHWA/NCEER Workshop on the National Representation of Seismic Ground Motion for New and Existing Highway Facilities*, Burlingame, California, May.

Teran-Gilmore, A. (1998), "A parametric approach to performance-based numerical seismic design", *Earthq. Spectra*, **14**(3), 501-520.

Uang, C.M. and Bertero, V.V. (1997), "Seismic response of an instrumented 13-story steel frame building damaged in the 1994 Northridge earthquake", *Earthq. Spectra*, **13**(1), 131-148.

Uang, C.M. and Bertero, V.V. (1990), "Evaluation of seismic energy in structures", *Earthq. Eng. Struct. Dyn.*, **19**(1), 77-90.

Vafaei, D. and Eskandari, R. (2015), "Seismic response of mega buckling-restrained braces subjected to fling-step and forward-directivity near-fault ground motions", *Struct. Des. Tall Spec. Build.*, **24**(9), 672-686.

Vafaei, D. and Eskandari, R. (2016), "Seismic performance of steel mega braced frames equipped with shape-memory alloy braces under near-fault earthquakes", *Struct. Des. Tall Spec. Build.*, **25**(1), 3-21.

Vafaei, D., Shemshadian, M.E. and Zahrai, S.M. (2010), "Seismic behavior of BRB frames under near fault excitations", *9th US National and 10th Canadian Conference on Earthquake Engineering*.

Zhou, Y. and Li, H. (2013), "Analysis of a high-rise steel structure with viscous damped outriggers", *Struct. Des. Tall Spec. Build.*, **23**(13), 963-979.

ETABS, Version 15.1.0. (2015), Computers and Structures, Inc., Berkeley, California, USA.

ASCE/SEI 7-2010 (2010), Minimum design loads for buildings and other structures, American Society of Civil Engineers, Reston, VA.

CC